nature communications

Article

https://doi.org/10.1038/s41467-024-51114-1

NAD^+ deficiency primes defense metabolism via $^1O_2$-escalated jasmonate biosynthesis in plants

Received: 11 October 2023

Accepted: 29 July 2024

Published online: 06 August 2024

Check for updates

Yechun Hong[1,2,5], Zongjun Yu[1,5], Qian Zhou[1], Chunyu Chen[1], Yuqiong Hao[1,3], Zhen Wang[4], Jian-Kang Zhu[2], Hongwei Guo[1] & Ancheng C. Huang[1]

Nicotinamide adenine dinucleotide (NAD^+) is a redox cofactor and signal central to cell metabolisms. Disrupting NAD homeostasis in plant alters growth and stress resistance, yet the underlying mechanisms remain largely unknown. Here, by combining genetics with multi-omics, we discover that NAD^+ deficiency in *qs-2* caused by mutation in NAD^+ biosynthesis gene-*Quinolinate Synthase* retards growth but induces biosynthesis of defense compounds, notably aliphatic glucosinolates that confer insect resistance. The elevated defense in *qs-2* is resulted from activated jasmonate biosynthesis, critically hydroperoxidation of α-linolenic acid by the 13-lipoxygenase (namely LOX2), which is escalated via the burst of chloroplastic ROS-singlet oxygen ($^1O_2$). The NAD^+ deficiency-mediated JA induction and defense priming sequence in plants is recapitulated upon insect infestation, suggesting such defense mechanism operates in plant stress response. Hence, NAD homeostasis is a pivotal metabolic checkpoint that may be manipulated to navigate plant growth and defense metabolism for stress acclimation.

Plant survival relies on active and timely reprogramming of metabolism to accommodate growth and defense needs in a changing environment, which is manifested by allocation of restricted energy resources to growth (corresponding to primary) and defense (corresponding to secondary) metabolisms, yet how plants manage growth and defense tradeoffs is not fully understood. Although plant hormones are recognized key players and their interplays could direct plant growth and defense[1,2], mechanistic insights on how biosynthesis of phytohormones get initiated are still lacking. Nicotinamide adenine dinucleotide (NAD^+) is a co-enzyme essential for cell metabolism and redox homeostasis and has been implicated to affect plant growth and development and stress responses[3–5]. NAD homeostasis was previously linked to the biosynthesis or signal transduction of phytohormones, including abscisic acid (ABA) and salicylic acid (SA), thus contributing to plant abiotic stress resistance and defense[5,6]. Reduced NAD^+ content was found to couple with decreased abscisic acid (ABA) biosynthesis in *Arabidopsis thaliana*[7], potentially via affecting the electron supply for the functioning of key redox enzymes, such as ABA biosynthetic enzymes ABA1 and ABA2[5]. Disruption of NAD^+ biosynthesis in plants also resulted in abnormal response to environmental stresses and ABA hypersensitive phenotype[8]. In contrast, increased production of NAD^+ induced biosynthesis of salicylic acid (SA) and enhanced plant pathogen resistance[6,9]. However, mechanisms underlying how NAD homeostasis connects phytohormones in mediating plant growth and stress response remain unclear, with genetic evidences being fragmented primarily owing to the difficulty in obtaining fertile NAD^+ biosynthesis mutants.

[1]Shenzhen Key Laboratory of Plant Genetic Engineering and Molecular Design, SUSTech-PKU Institute of Plant and Food Science, Department of Biology, School of Life Sciences, Southern University of Science and Technology, Shenzhen 518055 Guangdong, China. [2]Institute of Advanced Biotechnology and School of Medicine, Southern University of Science and Technology, Shenzhen 518055, China. [3]Institute of Wheat Research, Shanxi Agricultural University, Linfen 041000 Shanxi, China. [4]School of Life Sciences, Anhui Agricultural University, Hefei 230036 Anhui, China. [5]These authors contributed equally: Yechun Hong, Zongjun Yu. e-mail: huangac@sustech.edu.cn

In plants, NAD^+ is synthesized via the de novo pathway starting from aspartic acid in chloroplast and the salvage pathway that recycles NAD^+ catabolic products as precursors for regeneration[10,11]. NAD^+ can be phosphorylated to form NADP, and reduced to form NADH and NADPH, respectively. All these together constitute the NAD pool. The NAD^+ derivatives and their ratios in this pool are critical for maintaining cell redox and metabolic homeostasis, disruption of which can have major impacts on biological processes such as photosynthesis, signal transduction, and stress responses[4,5,12]. To date, the metabolic basis and mechanisms underpinning the altered plant growth and defense phenotypes caused by NAD deficiency and dyshomeostasis remain largely unknown. Understanding how NAD homeostasis tunes plant metabolism to accommodate growth and defense could inform the development of better strategies for engineering plant metabolism for stress acclimation and sustainable agriculture. We previously isolated and characterized a NAD^+ deficient *A. thaliana* mutant named *qs-2* which carries a point mutation in the *Quinolinate Synthase* (*QS*) gene that is responsible for the de novo synthesis of NAD^+ precursor quinolinate (Supplementary Fig. 1a)[8]. This mutant suffers from NAD dyshomeostasis with lower content of NAD^+ and grows small compared with wild-type *A. thaliana* Col-0 plant[8]. As complete NAD biosynthesis knockout mutant is often embryo lethal[11,13], such NAD^+ deficient mutant provides an excellent avenue for studying the altered metabolism caused by NAD dyshomeostasis and how such changes give rise to plant growth and defense phenotypes.

Here, by combining multi-omics and genetics approaches, we found that deficiency in NAD^+ biosynthesis resulted in NAD dyshomeostasis and metabolic reprogramming, leading to induction of defense metabolism and biosynthesis of defense compounds in *qs-2*, with notable hyperaccumulation of glucosinolates (GSLs). We further showed that such metabolic rewiring was triggered by the burst of chloroplastic reactive oxygen species (ROS)—singlet oxygen ($^1O_2$) which co-opts with LOX2-catalyzed hydroperoxidation of α-linolenic acid to activate jasmonate (JA) biosynthesis. The elevated defense metabolism confers *qs-2* with enhanced insect resistance. Furthermore, insect infestation could result in NAD^+ depletion and JA-mediated defense activation in *Arabidopsis thaliana*, supporting the operation of such defense pathway in plant biotic stress response. Collectively, our work reveals NAD homeostasis as a metabolic checkpoint for priming defense metabolism via $^1O_2$ burst and JA biosynthesis activation, shedding light on how plants tune metabolism to accommodate growth and defense, especially in response to insect infestation.

Results

NAD^+ deficiency induces defense metabolism, hyper-accumulating glucosinolates (GSLs) in *A. thaliana*

To understand the impacts of NAD^+ deficiency on plant metabolism, we first performed transcriptomics and untargeted metabolomics analyses on the rosette leaves of 3-week-old *qs-2* and Col-0 plants grown in soil. This integrated multi-omics approach allows us to systematically probe the differences between *qs-2* and Col-0 at both the transcript and metabolite levels. We found that the NAD^+ deficient mutant *qs-2* harbors distinct transcriptome and metabolome from those of Col-0 as evident from the principal component analysis (PCA) (Supplementary Fig. 1b–d). Over 300 differentially expressed genes (DEGs, 30 down- and 296 up-regulated) were identified in *qs-2* compared with Col-0 (Supplementary Fig. 1e and Supplementary Data 1). Further functional enrichment by Kyoto Encyclopedia of Genes and Genomes (KEGG) (www.kegg.jp/kegg/kegg1.html) mapped these DEGs to major biological processes like tryptophan and secondary metabolisms (including phenylpropanoid, flavonoid and glucosinolate biosynthesis) (Fig. 1a and Supplementary Fig. 1f). Using liquid chromatography-tandem mass spectrometry (LC–MS)-based untargeted metabolomics analysis in both positive and negative ionization modes, we found that *qs-2* harbors a metabolome distinct from that of Col-0 (Supplementary Fig. 1b, c). More than 600 differentially accumulated compounds (DACs) between *qs-2* and Col-0 rosette leaves were identified, and can be mapped to metabolic processes such as tryptophan metabolism, steroid biosynthesis, glucosinolates biosynthesis, and flavone and flavonol biosynthesis with KEGG analysis (Fig. 1a and Supplementary Fig. 1g, h). Notably, glucosinolate biosynthesis was the most highly represented metabolic process at both transcript and metabolite levels from our integrated-omics analysis (Fig. 1a–c).

We next verified the expression of glucosinolate (GSL) biosynthetic genes and contents of representative GSLs in *qs-2* by qRT-PCR and targeted metabolomics analysis (Fig. 1b, c, Supplementary Fig. 2a–d and Supplementary Table 1). Consistent with transcriptome and untargeted metabolomics data, indolic [indole-3-methyl (I3M) and 4-methoxy-indol-3-ylmethyl (4MOI3M)] and aliphatic [3-butenyl (4BTEY) and 4-methylsulfinylbutyl (4MSOB)] GSLs were highly accumulated in the rosette leaves of *qs-2* (Fig. 1d–g and Supplementary Fig. 2e). Moreover, hyperaccumulation of GSLs in *qs-2* could be restored to levels similar to those in Col-0 by genetically complementing *QS* gene in *qs-2* background (Fig. 1d–g and Supplementary Fig. 2e), indicative of the important role of de novo NAD^+ synthesis in regulating GSL metabolism. Since NAD dyshomeostasis caused by the deficiency in de novo synthesis could be complemented by boosting the salvage pathway in cytosol[14], we exogenously supplemented NAD^+ biosynthesis precursor nicotinic acid (NA) to *qs-2* and examined if the altered metabolic profiles in *qs-2* could be restored after NA treatment. Our results showed that the reduced NAD^+ content and hyperaccumulation of GSLs in *qs-2* could all be rescued after NA treatment, so as the suppressed chlorophyll metabolism and "small" phenotype of *qs-2* (Fig. 1h–k and Supplementary Fig. 2f–l). These results further suggest that NAD homeostasis plays an important role in controlling defense and photosynthesis related growth metabolisms in *qs-2*.

Induced aliphatic GSLs accumulation enhances *Arabidopsis* insect resistance

GSLs are well-known defense compounds conferring a broad spectrum of anti-insect and anti-microbial activities to cruciferous plants[15–17]. To examine whether the increased levels of GSLs could improve *qs-2* resistance to insects, we first generated GSLs abolished lines by overexpressing *AtBGLU28*, which encodes typical myrosinase capable of hydrolyzing GSLs[18], in *qs-2* background. We obtained two BGLU28-OE/*qs-2* lines which accumulate significantly less GSLs, yet still grew small like *qs-2* (Fig. 2a and Supplementary Fig. 3a–c), suggesting that the increasing GSL levels may not be responsible for the growth phenotype of *qs-2*. We next grew Col-0, BGLU28-OE2/*qs-2* together with *qs-2* and the complementation line COM1 in the same pot and subjected them to insect (*Helicoverpa armigera*) infestation. Our results showed that the leaves of *qs-2* were the least damaged amongst the genotypes tested after 8 h of insect infestation, whereas those of BGLU28-OE2/*qs-2* exhibited significant damages (Supplementary Fig. 3d, e). This finding suggested that the high levels of GSLs in *qs-2* are responsible for deterring the insects (*H. armigera*). To exclude the effects of plant size on insect preference, we further fed the insects with sufficient leaves from the different plant genotypes and found that *qs-2* exhibited enhanced insect resistance as insects fed on *qs-2* leaves grew significantly smaller than those on Col-0 ones (Fig. 2b, c). Moreover, such enhanced resistance was restored in BGLU28-OE2/*qs-2* or *QS* complementation plants COM1 (Fig. 2b, c), substantiating the increased GSL levels in *qs-2* can confer plant insect resistance.

Since both aliphatic and indolic GSLs are highly accumulated in *qs-2*, we sought to further uncover which type of GSLs contribute predominantly to the insect resistance of *qs-2*. To this end, we used

https://doi.org/10.1038/s41467-024-51114-1

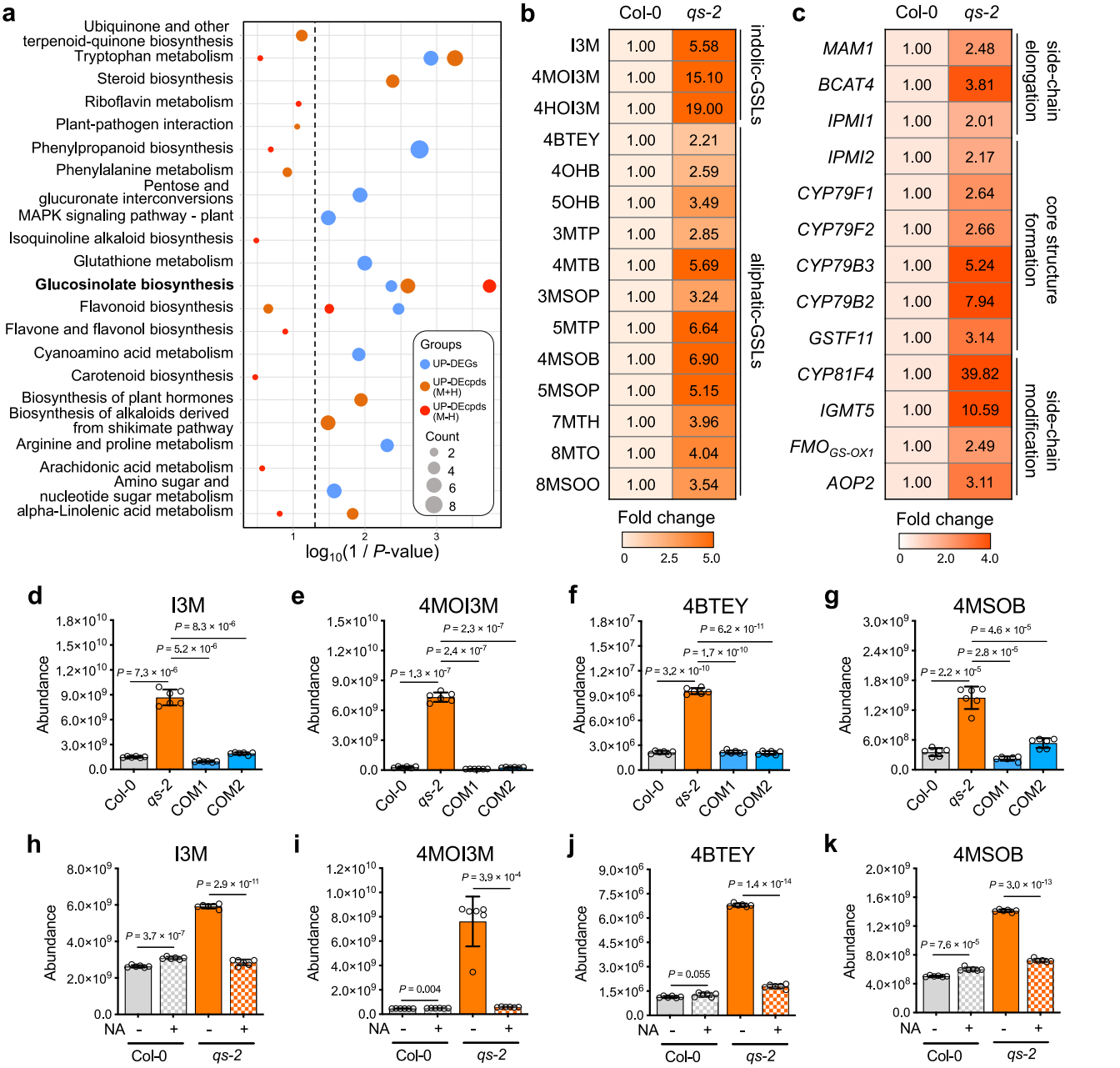

Fig. 1 | NAD⁺ deficiency induced biosynthesis of glucosinolates (GSLs) in rosette leaves of *qs-2*. **a** Integrated KEGG analysis of differentially expressed genes and accumulated compounds between Col-0 and *qs-2* collectively indicate the significant induction of glucosinolate biosynthesis in *qs-2*. *p* values are calculated with the cumulative hypergeometric distribution by comparing the number of compounds in the set and in the background with a given annotation. Resulting *p* values are adjusted for multiple testing using the Benjamini–Hochberg adjusted *p* values method. Blue dots: upregulated genes (UP-DEGs); Orange dots: upregulated compounds detected in positive mode [(UP-DEcpds $(M+H)^+$)]; Red dots: upregulated compounds detected in negative mode [(UP-DEcpds $(M-H)^-$)]. Comparison of key aliphatic and indolic GSL contents (**b**) and GSL biosynthetic gene transcripts (**c**) in leaves of Col-0 and *qs-2*. Heatmaps indicate fold change in *qs-2* vs. Col-0. Relative contents of indolic-GSLs I3M (**d**) and 4MOI3M (**e**), aliphatic-GSLs 4BTEY (**f**) and 4MSOB (**g**) determined in the rosette leaves of 21-day-old Col-0, *qs-2*, COM1 and COM2. Each bar represents the means ± SD ($n = 6$), and the significance analysis was performed by two-tailed Student's *t* test. Relative contents of I3M (**h**), 4MOI3M (**i**), 4BTEY (**j**) and 4MSOB (**k**) in Col-0 and *qs-2* with and without nicotinic acid (NA) treatment. Fourteen-day-old Col-0 and *qs-2* mutant plants grown in soil were supplemented with 1 mM NA for additional 7 days before determination. The values represented the means ± SD ($n = 6$), two-sided Student's *t* test. Source data are provided as a Source Data file.

CRISPR-Cas9 method to mutate the known transcription factors regulating aliphatic (*MYB28* and *MYB29*)[19] or indolic (*MYB34* and *MYB51*) GSL biosynthesis[20], respectively, and successfully obtained triple mutants accumulating mainly aliphatic (*qs-2myb3451*) or indolic (*qs-2myb2829*) GSLs (Fig. 2d and Supplementary Fig. 3f, g). Intriguingly, we found that abolishing aliphatic GSLs alone in the triple mutant *qs-2myb2829* could eliminate the insect resistance phenotypes of *qs-2*, in stark contrast, depriving indolic GSLs (in *qs-2myb3451*) could not (Fig. 2e, f). Together with the phenotypes of BGLU28-OE/*qs-2* observed under insect treatments, our results collectively suggest that elevated aliphatic GSLs likely play a dominant role in boosting *Arabidopsis* insect (*H. armigera*) resistance as seen in *qs-2*.

https://doi.org/10.1038/s41467-024-51114-1

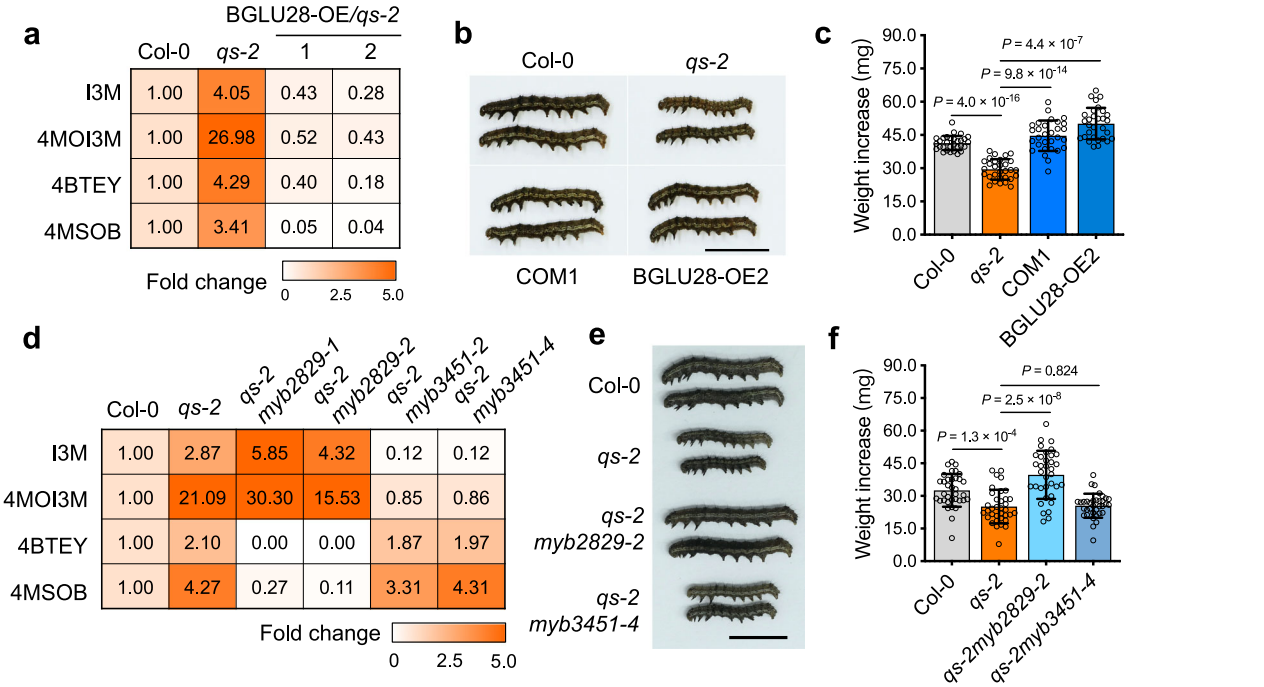

Fig. 2 | Hyperaccumulation of glucosinolates conferred *A. thaliana* resistance to insect attack. a Heatmap of the relative contents of four key glucosinolates in the rosette leaves of Col-0, *qs-2* and two lines BGLU28-OE1/*qs-2* and BGLU28-OE2/*qs-2* overexpressing BGLU28 in *qs-2* background. **b** Phenotype of *H. armigera* fed with leaves of Col-0, *qs-2*, COM1, and BGLU28-OE2/*qs-2*. Scale bar, 1 cm. **c** Weight increase of *H. armigera* larvae fed with plant leaves indicated in (**b**). The data represent means ± SD ($n = 30$), two-sided Student's *t* test. **d** A heatmap showing the relative contents of four key GSLs in the rosette leaves of *qs-2*, two independent *qs-2myb2829* and *qs-2myb3451* lines and Col-0 wild-type plants. **e** Images of *H. armigera* fed with *qs-2*, *qs-2myb2829-2*, *qs-2myb3451-4* and Col-0 plants. Bar, 1 cm. **f** Quantification of weight increase of *H. armigera* larvae fed with plants of indicated genotypes were shown in (**e**). The data are means ± SD ($n = 35$), and the significance analysis was performed by two-tailed Student's *t* test. Source data are provided as a Source Data file.

NAD homeostasis mediates plant growth and defense tradeoffs through JA-dependent metabolic reprogramming

We next asked how NAD^+ deficiency induced GSL biosynthesis. In our transcriptomic analysis, response to jasmonic acid was highly represented in the GO term enrichment analysis (Supplementary Fig. 4a, b). Moreover, biosynthesis and metabolism of defense metabolites GSLs are known to be regulated by phytohormone JAs[21–23]. Further qRT-PCR analysis confirmed that several well-known JA responsive genes including *THI2.1*, *PDF1.2* and *VSP1*, were upregulated in *qs-2*, indicative of activation of JA signal transduction (Supplementary Fig. 4c–e). These results indicate that NAD dyshomeostasis caused by deficient biosynthesis may induce GSL biosynthesis via JA signal transduction.

To verify our hypothesis, we genetically blocked JA signal transduction and biosynthesis in *qs-2* by crossing the JA receptor mutant *coi1-2*[24] with *qs-2* to generate double mutant *qs-2coi1-2* and CRISPR-Cas9-mediated knockout of JA biosynthetic gene *Allene Oxide Synthase* (*AOS*)[25] to generate double mutant *qs-2aos*, respectively (Fig. 3a and Supplementary Fig. 4f, g). Transcript levels of selected JA responsive marker genes and the contents of JA and jasmonoyl-isoleucine (JA-Ile) diminished in the generated double mutants *qs-2coi1-2* and *qs-2aos* (Supplementary Fig. 4h–l). These two double mutants both contain significantly lower amounts of aliphatic and indolic GSLs, with levels comparable to those in *A. thaliana* wild-type Col-0 plants (Fig. 3b). Importantly, the double mutants grew significantly larger and were less tolerant to insect infestation than *qs-2* (Fig. 3c–e), suggesting that blocking JA signal transduction and biosynthesis could rescue both growth and defense phenotypes of *qs-2* to a great extent, possibly by shunting metabolic flux from the induced defense metabolism back toward growth one. Therefore, we conclude that NAD homeostasis could modulate plant growth and defense and its deficiency escalates plant defense via activation of JA-dependent metabolism, notably GSL biosynthesis.

LOX2-catalyzed hydroperoxidation activates JA biosynthesis upon NAD^+ deficiency

It is intriguing that activation of JA-dependent metabolism accounts considerably for the growth and defense phenotypes of *qs-2* (Fig. 3), yet how NAD^+ deficiency initiates JA biosynthesis and signaling remains unclear. To further unveil the intrinsic links between NAD^+ and JA in *A. thaliana*, we sought to obtain a full picture of the JA biosynthesis dynamics via determining the contents of key precursors and intermediates in the JA biosynthetic pathway[26], including α-linolenic acid (α-LeA), 13(S)-hydroperoxide (13-HPOT), 12-oxo-phytodienoic acid (12-OPDA), JA (referred to (+)-7-*iso*-JA) and JA-Ile (referred to (+)-7-*iso*-JA-Ile) in the leaves of *qs-2* and the complementation lines COM1 and COM2 (Fig. 4a–f). Interestingly, we found that the content of α-LeA decreased significantly whereas those of the downstream products 13-HPOT, 12-OPDA, JA and JA-Ile increased substantially in *qs-2* compared with Col-0 (Fig. 4b–f), suggesting that activation of JA biosynthesis may be initiated from the conversion of α-LeA to 13-HPOT.

In *A. thaliana*, there are four *13-LOX* genes encoding non-heme iron-containing dioxygenases 13-lipoxygenases to convert α-LeA to 13-HPOT, amongst which *LOX2* shows strongest expression in rosette leaves—the tissue we selected for investigation in this study (Supplementary Fig. 5a)[27,28]. The expressions of *LOX2* and three other JA biosynthetic genes were all highly expressed in *qs-2* (Fig. 4g and Supplementary Fig. 5b–d). Further immunoblotting analysis confirmed that LOX2 protein was highly accumulated in *qs-2* mutant (Fig. 4h), indicative of LOX2 as a likely key 13-LOX responsible for α-LeA reduction in *qs-2*. To further delineate the role of LOX2 in the hyperaccumulation of JA and GSLs in *qs-2*, we generated *LOX2* CRISPR-knockout mutant in both Col-0 and *qs-2* backgrounds and obtained single and double mutants *lox2-c1/2* and *qs-2lox2-c1/2*, respectively (Fig. 4i and Supplementary Fig. 5e). Loss of *LOX2* in both Col-0 (*lox2-c1* and *lox2-c2*) and *qs-2* (*qs-2lox2-c1* and *qs-2lox2-c2*) resulted in markedly

https://doi.org/10.1038/s41467-024-51114-1

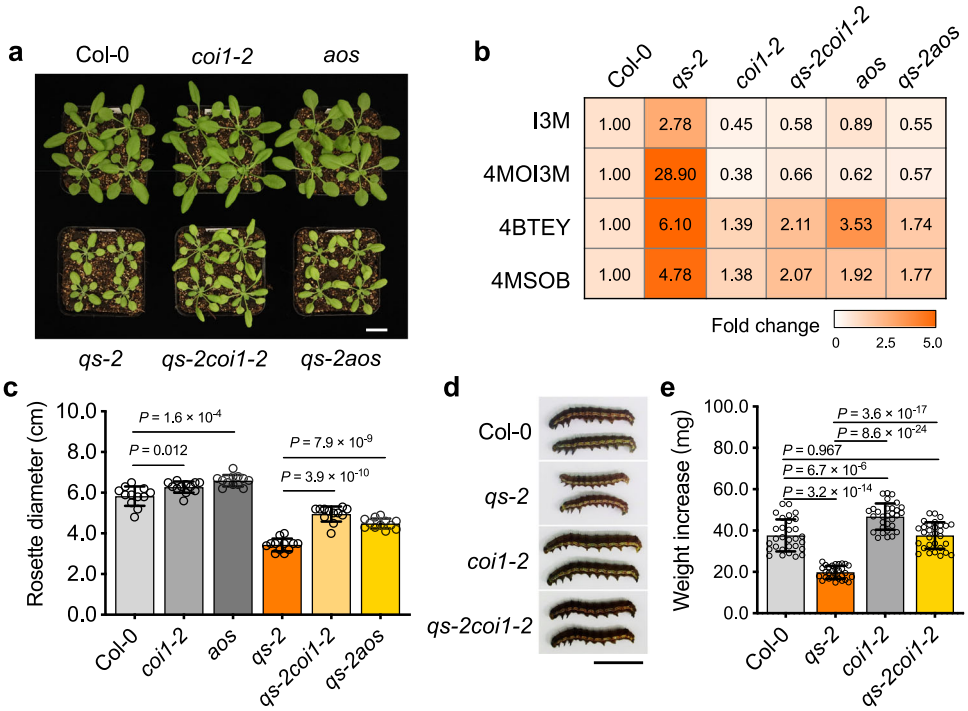

Fig. 3 | NAD$^+$ deficiency-induced GSL hyperaccumulation and enhanced resistance to insects in *A. thaliana* is dependent on JA signal transduction. **a** Phenotypes of 21-day-old Col-0, *qs-2*, *coi1-2*, *qs-2coi1-2*, *aos* and *qs-2aos* plants grown in soil. Scale bar, 2 cm. **b** Heatmap of the relative contents of four key GSLs in the rosette leaves of Col-0, *qs-2*, *coi1-2*, *qs-2coi1-2*, *aos* and *qs-2aos* plants. **c** Rosette diameter of the *A. thaliana* lines depicted in (**a**). Each bar represents the means ± SD ($n = 12$), two-sided Student's *t* test. **d** Image of *H. armigera* fed with *qs-2*, *coi1-2*, *qs-2coi1-2* and Col-0 plants. Bar, 1 cm. **e** Weight increase of *H. armigera* larvae fed with leaves of Col-0, *qs-2*, *coi1-2* and *qs-2coi1-2* plants. Shown here are means ± SD ($n = 30$), and the significance analysis was performed by two-tailed Student's *t* test. Source data are provided as a Source Data file.

reduced JA content with hyperaccumulation of α-LeA (Fig. 4j–m), and GSL levels in *qs-2* restored to those in Col-0 (Fig. 4n). Therefore, mutating *LOX2* alone is sufficient to rescue the induced defense metabolism in *qs-2*, supporting that LOX2 is a prominent driver for the enhanced biosynthesis of JA and GSLs in *qs-2*. Furthermore, we found that blocking JA signal transduction in Col-0 and *qs-2* backgrounds, i.e., *coi1-2* and *qs-2coi1-2*, could also markedly down-regulate JA biosynthetic genes (Supplementary Fig. 5g–j), leading to significant reduction of 13-HPOT, 12-OPDA and JA in *qs-2coi1-2* compared with *qs-2* (Supplementary Fig. 5k–n). This indicates that positive feedback regulation on JA biosynthesis by JA signaling[29,30] plays important roles in the signal cascade of NAD$^+$ deficiency-activated JA biosynthesis.

NAD$^+$ deficiency-induced $^1O_2$ burst co-opts with LOX2 to initiate JA biosynthesis

NAD dyshomeostasis-induced ROS (H_2O_2 and O_2^-) overaccumulation was previously shown to play a role in plant salt stress tolerance and pathogen resistance via potential interplays with the biosynthesis or signal transduction of phytohormones ABA and SA[5–8]. It's possible that NAD$^+$ deficiency-induced ROS production may also have a role in activating JA biosynthesis. To verify our hypothesis, we first examined the roles of H_2O_2 and O_2^- in *qs-2* with chemical (NA) treatment or genetic manipulations (*QS* complementation line COMs, and *qs-2coi1-2*). Our results showed that both types of ROS could be rescued by genetic complementation or NA supplement but not *coi1-2* mutation, suggesting that NAD$^+$ deficiency-induced ROS accumulation is independent of JA signaling pathway (Supplementary Fig. 6a–c). Next, we wondered if activation of JA biosynthesis in *qs-2* could be restored when H_2O_2 and O_2^- were cleaned in the *qs-2* background. We then determined the levels of JA and JA-related compounds in the previously generated ROS mutant *qs-2rbohF3*[8], where the plasma membrane NADPH oxidase gene *RBOHF* responsible for the generation of H_2O_2 and O_2^- was mutated in *qs-2* background and H_2O_2 and O_2^- were mostly removed (Supplementary Fig. 6d). Interestingly, we found that the contents of JA and its biosynthetic precursors in *qs-2rbohF3* remain at levels similar to those in *qs-2* (Fig. 5a–e), so as both indolic and aliphatic GSLs (Fig. 5f). This suggests that high levels of H_2O_2 and O_2^- do not contribute to the activation of JA biosynthesis and downstream defense metabolism in *qs-2*.

Considering *qs-2* has small rosettes and lower chlorophyll contents (Supplementary Fig. 2f–h), it is likely that photosynthesis of *qs-2* is impaired. To verify this, we determined the maximum photochemical efficiency of PSII (*Fv*/*Fm*) in *qs-2*, COM1 and Col-0 wild-type plants and found that the *Fv*/*Fm* value in *qs-2* rosette leaves was indeed significantly lower than those of the other two genotypes (Fig. 5g). Because malfunction of photosynthesis often results in the production of another type of ROS-singlet oxygen ($^1O_2$) in chloroplast[31], we next determined the levels of $^1O_2$ in the different mutant lines we have generated. Using a fluorescent probe Singlet Oxygen Sensor Green (SOSG) highly selective for $^1O_2$[32], we could detect strong green fluorescent signals in the leaves of *qs-2* but not Col-0, suggesting that $^1O_2$ was highly enriched in *qs-2* (Fig. 5h). Furthermore, $^1O_2$ burst in *qs-2* could be restored in the complementation plants COM1/2 and by exogenous NA supplementation (Fig. 5h and Supplementary Fig. 7a), which is accompanied with resetting of the hyperaccumulation of JA and JA-Ile (Supplementary Fig. 7b, c). To this point, our results substantiate that $^1O_2$ burst and enhanced JA biosynthesis in *qs-2* are due to NAD$^+$ deficiency and sequential dyshomeostasis.

Next, we further examined if the enriched $^1O_2$ has a role in JA biosynthesis activation. Because $^1O_2$ was still enriched in the double mutant *qs-2rbohF3* (Fig. 5h), this makes *qs-2rbohF3* the mutant line accumulating only $^1O_2$ without H_2O_2 and O_2^- (Fig. 5i). We then sought to reduce the $^1O_2$ level in *qs-2rbohF3* to examine if this impacts JA biosynthesis. We exogenously applied 4,5-Dihydroxy-1,3-

https://doi.org/10.1038/s41467-024-51114-1

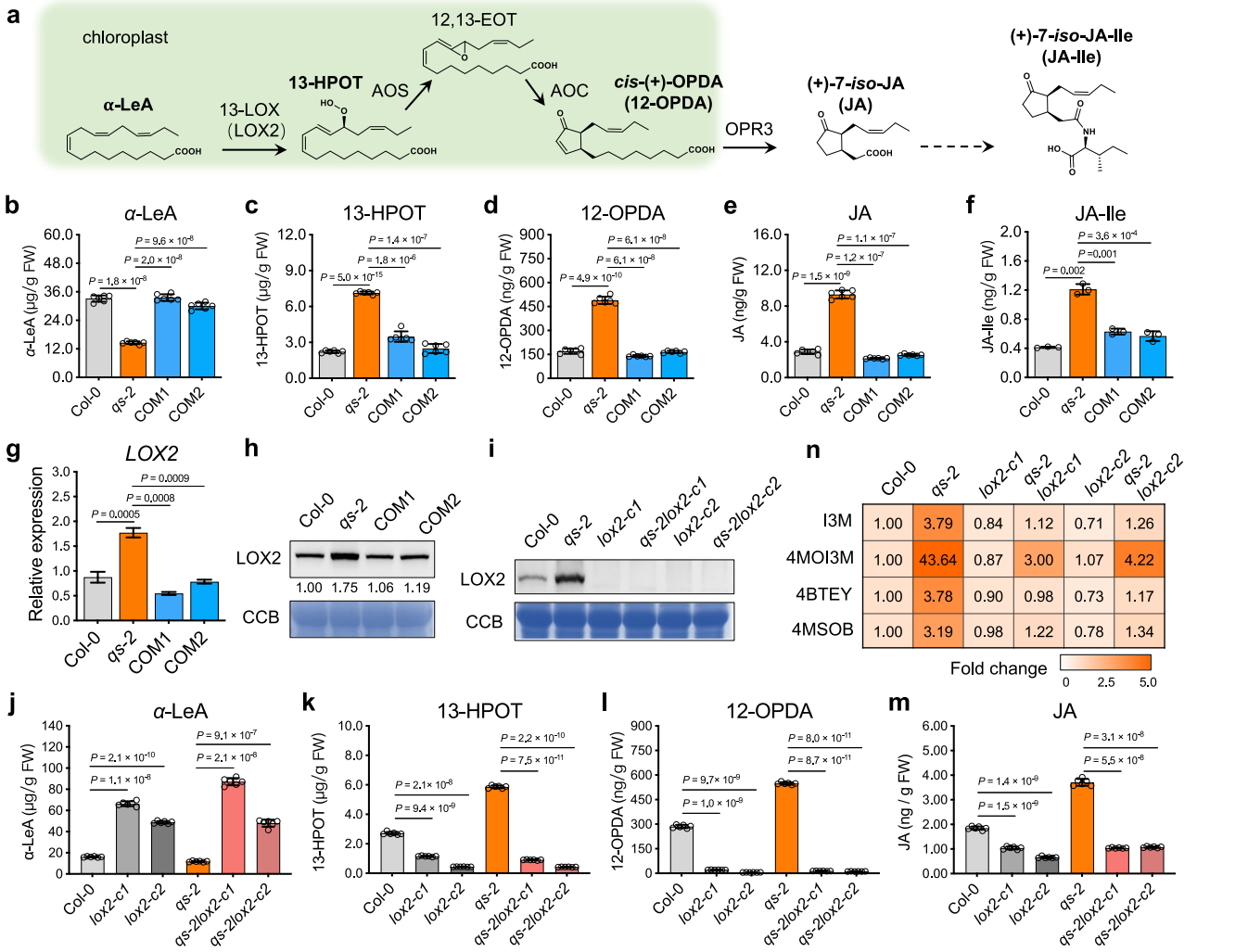

Fig. 4 | *LOX2* is the key for NAD⁺ deficiency-induced jasmonate biosynthesis. **a** Overview of upstream JA biosynthesis pathway from α-LeA to12-OPDA in chloroplast. Contents of α-LeA (**b**), 13-HPOT (**c**), 12-OPDA (**d**), JA (**e**) and JA-Ile (**f**) in the leaves of Col-0, *qs-2*, COM1 and COM2 plants. The data represent the means ± SD ($n = 6$, $n = 3$ for JA-Ile), two-sided Student's *t* test). **g** The transcript level of *LOX2* in *qs-2*, two complementation lines COM1 and COM2, and wild-type Col-0. *ACT2* was used as internal control. The values represented the means ± SD ($n = 3$), and the significance analysis was performed by two-tailed Student's *t* test. **h** Immuno-blotting of LOX2 protein from Col-0, *qs-2*, COM1 and COM2 plants. The Coomassie blue (CCB) staining was used as the loading control. **i** Immuno-blotting of LOX2 protein in Col-0, *qs-2*, *lox2-c1*, *lox2-c2*, *qs-2lox2-c1* and *qs-2lox2-c2* plants. Contents of α-LeA (**j**), 13-HPOT (**k**), 12-OPDA (**l**) and JA (**m**) in *qs-2*, two *lox2* single mutants and two *qs-2lox2* double mutants. The data represent the means ± SD ($n = 6$), and the significance analysis was performed by two-tailed Student's *t* test. **n** A heatmap showing the relative contents of four key GSLs in the rosette leaves of above-mentioned materials. Source data are provided as a Source Data file.

benzenedisulfonic acid disodium salt monohydrate (DBS), an effective $^1O_2$ scavenger structurally similar to vitamin E[33,34], to the rosette leaves of *qs-2rbohF3* and found that the $^1O_2$ level in *qs-2rbohF3* could be repressed by DBS treatment (Supplementary Fig. 7d). The reduction of $^1O_2$ level in *qs-2rbohF3* after DBS treatment was coupled with significant decrease of 13-HPOT, 12-OPDA and JA levels in *qs-2rbohF3* (Supplementary Fig. 7f–h), albeit the level of α-LeA didn't change much after DBS treatment (Supplementary Fig. 7e). These results suggest that hyperaccumulation of $^1O_2$ likely co-opts with LOX2-mediated hydroperoxidation of α-LeA and enhanced production of 13-HPOT to facilitates JA biosynthesis.

Since LOX2-catalyzed hydroperoxidation of α-LeA involves free radicals potentially derived from $^1O_2$[35], and LOX2 is the key to NAD⁺ deficiency-activated JA biosynthesis (*vide supra*), we next determined its protein level in the JA and ROS related mutant lines. We found that LOX2 protein was highly accumulated in both *qs-2* and *qs-2rbohF3*, whilst lowly accumulated in both *coi1-2* and *qs-2coi1-2* (Supplementary Fig. 7i, j). Intriguingly, we found that *qs-2coi1-2* contains higher level of $^1O_2$ and 13-HPOT than those in *coi1-2* even when LOX2 is lowly accumulated (Supplementary Figs. 5j and 7k), supporting that the elevated chloroplastic $^1O_2$ is critical for activating JA biosynthesis (Supplementary Fig. 7c, d). To further demonstrate the core role of $^1O_2$-LOX2 cascade in mediating JA biosynthesis, we exogenously supplemented 3-(3,4-dichlorophenyl)-1,1-dimethylurea (DCMU), which triggers $^1O_2$ production by blocking plastoquinone reduction in PSII[32], to Col-0 wild-type and *lox2-c1* mutant followed by determining the contents of JA-related compounds. We found that the contents JA-related compounds increased significantly after 6 h of DCMU treatment, then decreased after 12 h in both Col-0 and *lox2-c1* (Fig. 5j–n). Loss of *LOX2* resulted in significantly high accumulation of α-LeA and low levels of the JA biosynthesis pathway downstream products (Fig. 5j–n), suggesting that LOX2 is indeed the core 13-LOX in $^1O_2$-mediated JA biosynthesis in rosette leaves. Furthermore, enzymatic $^1O_2$-mediated peroxidation of polyunsaturated fatty acids was previously observed[36], supporting that $^1O_2$ co-opts with LOX2 to activate JA biosynthesis upon NAD⁺ deficiency.

https://doi.org/10.1038/s41467-024-51114-1

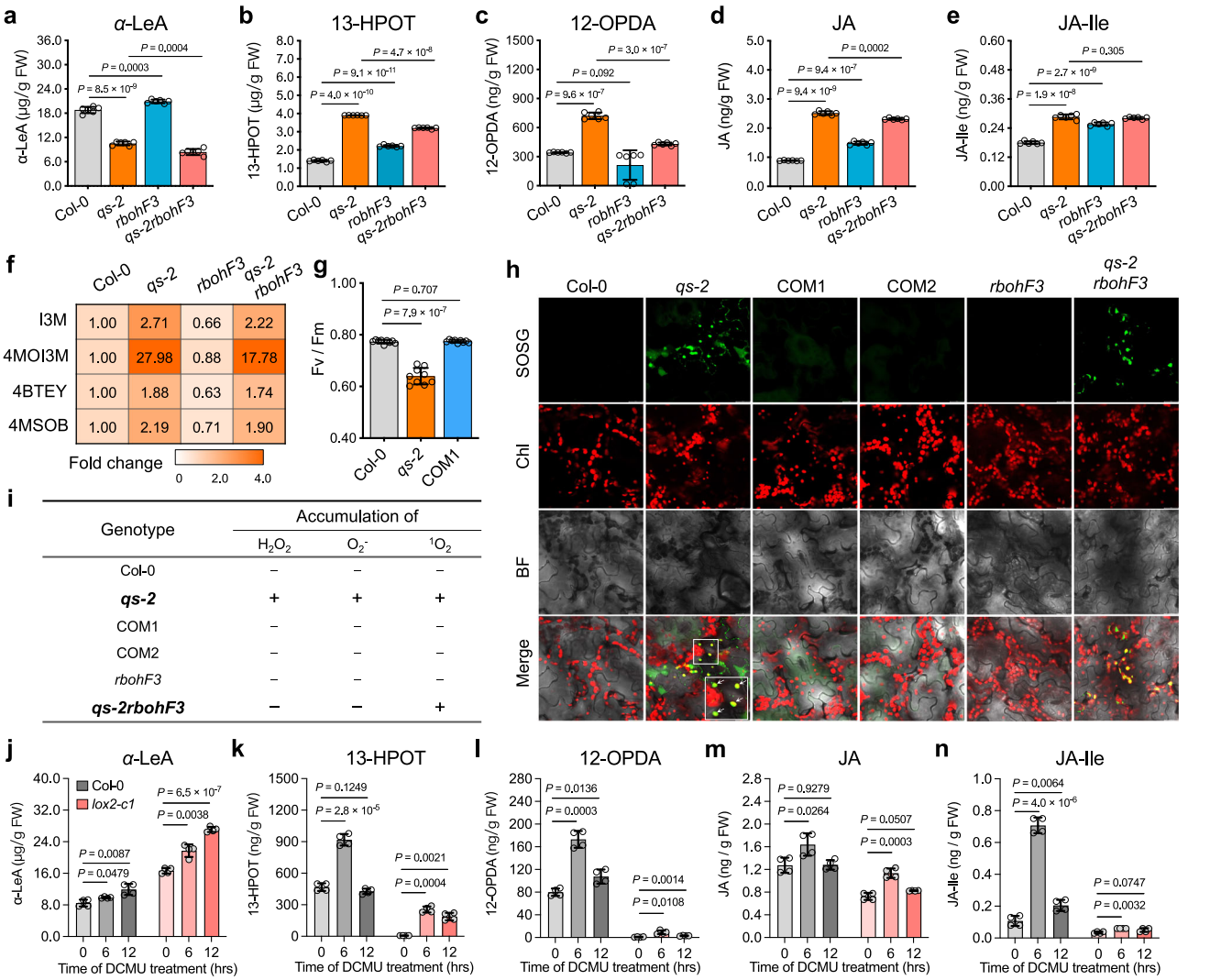

Fig. 5 | Chloroplastic $^1O_2$ burst upon NAD$^+$ depletion activates jasmonate biosynthesis. Contents of α-LeA (**a**), 13-HPOT (**b**), 12-OPDA (**c**), JA (**d**) and JA-Ile (**e**) in the leaves of Col-0, *qs-2*, *rbohF3* and *qs-2rbohF3* plants. The data represent the means ± SD ($n = 6$ biological replicates), two-sided Student's *t* test. **f** A heatmap showing the relative contents of four key GSLs in the rosette leaves of Col-0, *qs-2*, *rbohF3* and *qs-2rbohF3* plants. **g** Analysis of maximum photochemical efficiency of PSII (*Fv*/*Fm*) in *qs-2* mutant, COM1 and Col-0 wild-type plants. The *qs-2*, COM1 and Col-0 plants were grown in soil under normal growth conditions for 21 days, then the mature rosette leaves were analyzed by a portable fluorometer (JUNIOR-PAM, Walz, Germany). $n = 9$, two-sided Student's *t* test. **h** Representative confocal images showing SOSG fluorescence in leaf mesophyll cells of 3-week-old Col-0, *qs-2*, COM1, COM2, *rbohF3* and *qs-2rbohF3* plants. Scale bars, 20 μm. **i** Summary of the accumulation of different ROSs in the rosette leaves of indicated genotypes. Contents of α-LeA (**j**), 13-HPOT (**k**), 12-OPDA (**l**), JA (**m**) and JA-Ile (**n**) in the leaves of Col-0 and *lox2-c1* with DCMU treatment for indicated hours. The data represent the means ± SD ($n = 4$), and the significance analysis was performed by two-tailed Student's *t* test. Source data are provided as a Source Data file.

NAD homeostasis is a critical metabolic checkpoint for tuning growth and defense in plant stress response

To further examine whether NAD$^+$ deficiency-mediated JA activation operates in plant stress response, we first subjected *A. thaliana* Col-0 and *coi1-2* plants to insect infestation and performed metabolite profiling (Fig. 6a–e and Supplementary Fig. 8a–d). We found that the NAD$^+$ content deceased significantly in the leaves of Col-0 plants treated with insects (Fig. 6b), while its reduced form NADH or phosphorylated form NADP(H) showed little changes after this treatment (Fig. 6c–e). Interestingly, such insect infestation-induced NAD$^+$ depletion could also be observed in *coi1-2* plants (Supplementary Fig. 8a), indicating that insect attack-induced NAD dyshomeostasis happens upstream of JA signaling pathway. Furthermore, insect infestation also enhanced $^1O_2$ production, supporting that NAD$^+$ reduction could trigger $^1O_2$ accumulation during insect infestation (Fig. 6f). Sequentially, JA, JA-Ile and the defense metabolites GSLs were accumulated after insect infestation (Fig. 6g, h and Supplementary Fig. 8e). Collectively, our results suggest that the NAD$^+$ deficiency-induced defense pathway functions in *A. thaliana*'s response to insect infestation. We also determined the transcript levels of four *13-LOX*s upon insect infestation, and the results showed that *LOX2* was the most significantly upregulated *13-LOX* gene upon insect attack amongst the four tested (Supplementary Fig. 8f). In addition, JA accumulation in leaves triggered by insect infestation was largely repressed in *lox2-c1* mutant compared with Col-0 wild-type plants, substantiating that *LOX2* is the key component in insect attack-induced JA biosynthesis (Supplementary Fig. 8g).

Although it is not yet clear what triggers NAD$^+$ depletion under insect infestation, endogenous NADases are known to be able to degrade NAD$^+$ and may result in NAD$^+$ depletion[37,38]. To better verify the effects of NAD$^+$ depletion on JA biosynthesis, we overexpressed the TIR domain of mammalian SARM1 protein (namely HsSARM1-TIR),

https://doi.org/10.1038/s41467-024-51114-1

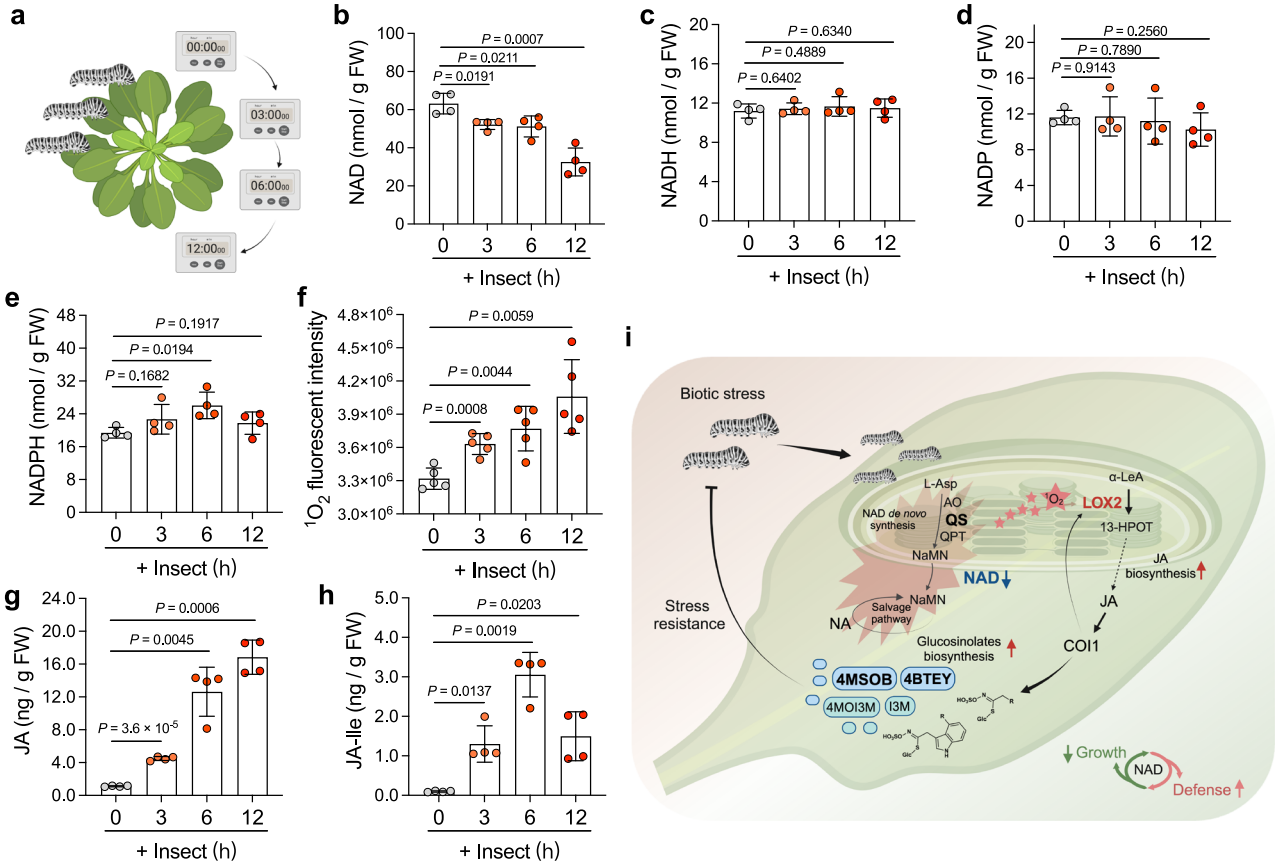

Fig. 6 | NAD dyshomeostasis resulted from insect infestation activates jasmonate biosynthesis for plant defense priming. a A schematic for the metabolite analysis of plant under insect infestation. The contents of NAD^+ (**b**), NADH (**c**), NADP (**d**) and NADPH (**e**) in rosette leaves of Col-0 wild-type plant under insect infestation. Each bar represents the means ± SD ($n = 4$ biological replicates), and the significance analysis was performed by two-sided Student's *t* test. **f** Determination of $^1O_2$ level in rosette leaves of Col-0 wild-type plant under insect infestation for indicated hours. $n = 5$, two-sided Student's *t* test. The contents of JA (**g**) and JA-Ile (**h**) in the leaves of Col-0 under insect infestation. The data represent the means ± SD ($n = 4$), two-sided Student's *t* test. **i** A proposed model showing the activation and operation of NAD^+-depletion defense pathway in response to biotic stress. Source data are provided as a Source Data file. **a** and **i** are created with BioRender.com released under a Creative Commons Attribution-NonCommercial-NoDerivs 4.0 International license (https://creativecommons.org/licenses/by-nc-nd/4.0/deed.en).

which previously exhibited strong hydrolyzing activity toward NAD^+ without producing immunity-related NAD^+ degradation products pRib-AMP or pRib-ADP, in leaves of *Nicotiana benthamiana* (Supplementary Fig. 8h, i)[37,38]. As expected, transient expression of HsSARM1-TIR protein reduced NAD^+ content gradually along with the production of its degradation product cADPR in *N. benthamiana* leaves (Supplementary Fig. 8j, k). Importantly, the $^1O_2$, JA and JA-Ile levels were significantly increased in *N. benthamiana* leaves expressing HsSARM1-TIR even in 24H (24 h) when NAD^+ reduction was ~40%, suggesting that mild NAD^+ deficiency may already be capable of inducing $^1O_2$ production and JA biosynthesis in plants (Supplementary Fig. 8l–n). This result is consistent to the NAD^+ reduction and defense activation sequence we observed in our insect infestation experiments (*vide supra*), further supporting that the NAD^+ deficiency induced defense mechanism operates in insect infestation. Given that HsSARM1-TIR also possesses a lower but significant ability to hydrolyze NADP[38], we further determined the contents of other pyridine nucleotides in HsSARM1-TIR-expressed tobacco leaves. In contrast to the substantial depletion of NAD^+ after HsSARM1-TIR expression, the contents of NADH and NADP decreased to a much less extent with NADPH remaining relatively stable 48 h' post infiltration (Supplementary Fig. 8o–q), suggesting that NAD^+ functions as the key pyridine nucleotide in HsSARM1-TIR-induced $^1O_2$ production and JA biosynthesis. Taken together, our findings reveal that NAD homeostasis is a critical checkpoint for navigating plant growth and defense metabolism in plant stress response (Fig. 6i).

Discussion

NAD homeostasis controls redox signaling and its interplay with phytohormone biosynthesis or signal transduction are critical for plant growth and development and adaption[4,5]. Compared to the previously established connection between NAD homeostasis and phytohormone ABA during plant response to abiotic stress[5,8], we revealed here that NAD homeostasis connects JA biosynthesis and signal transduction to prime defense metabolism in plants' response to insect infestation (Figs. 2 and 3). The burst of ROSs generated upon NAD^+ deficiency can exert various functions in connection with phytohormone signaling[5,8], and we demonstrated that chloroplastic $^1O_2$, rather than H_2O_2 and O_2^-, acts specifically to initiate JA biosynthesis in leaf tissue (Fig. 5). More importantly, burst of chloroplastic $^1O_2$ co-opts with LOX2-mediated hydroperoxidation of α-LeA, thus making $^1O_2$-LOX2 an important cascade in escalating JA biosynthesis (Fig. 5 and Supplementary Fig. 7). Being the central phytohormone in plant defense, the biosynthesis and signal transduction pathways of jasmonates are conserved in plants, whilst the JA-regulated end defense compounds are taxonomically and functionally specific, such as GSLs in cruciferous plants. Both indolic and aliphatic GSLs could be induced by insect attack with the latter one found to exhibit inhibition against broader range of insects[39,40].

The aliphatic or indolic GSLs deficient mutant used in previous studies were *cyp79f1f2* and *cyp79b2b3*, both of which were biosynthetic mutants exhibiting severe growth phenotypes, thus making it difficult to distinguish their specific functions[41,42]. By generating mutants accumulating only aliphatic (*qs-2myb3451*) or indolic (*qs-2myb2829*) GSLs without altering plant growth, our study provides strong genetic evidences to support that aliphatic GSLs play more dominant roles than the indolic ones in insect resistance, especially against *H. armigera* (Fig. 2e, f). The sequence of NAD^+ deficiency-induced JA-dependent defense metabolic reprogramming indicates that NAD homeostasis can be a target for metabolic engineering for improved plant biotic stress resilience (Fig. 6e).

The NAD^+ deficiency-triggered JA-related defense pathway may function extensively to provide basal defense when plants encounter insect attack, as significant decrease of NAD^+ content rather than other NAD^+ derivatives was detected upon insect infestation (Fig. 6 and Supplementary Fig. 8). The specific depletion of NAD^+ (as opposed to its derivatives) caused by insect infestation may serve as a relatively precise defense response trigger in plants. In contrast to NAD^+ depletion, over-production of NAD^+ via expressing bacterial *NadC* gene, which encodes the NAD^+ biosynthetic enzyme quinolinate phosphoribosyltransferase, could enhance SA and ROS production in *Arabidopsis* and consequently improve plant pathogen resistance, suggesting that NAD^+ level is crucial for maintaining NAD homeostasis and tuning plant defense[6]. The elevated NAD^+-induced ROS accumulation is more likely linked to mitochondrial metabolism upon pathogen infection and not related to RBOHs[6,43], whereas NAD^+ deficiency triggers H_2O_2 and O_2^- accumulation in a RBOHF-dependent manner (Supplementary Fig. 6g, h)[8], and can cause chloroplastic $^1O_2$ production coupled with JA biosynthesis activation (Figs. 5 and 6). The NAD^+ deficiency triggered defense activation characterized in the *qs-2* mutant could be effectively recapitulated by degrading NAD^+ via expressing the NAD^+-hydrolyzing TIR protein in *N. benthamiana* leaves[37,38] (Supplementary Fig. 8h–q). Therefore, the insect infestation-triggered NAD^+ decrease is potentially also a result of NADase action, though it's not yet clear whether such NADase activity derives from insects or plants, which remains an open question for future investigation. At this point, it's evident that NAD homeostasis is tightly coupled with changing environmental stresses and enables plants to tune its defense strategy, intensity and selectivity. In addition, NAD^+ depletion-induced defense is likely to accompany with compromised photosynthesis and metabolic channeling and flux diverting from growth metabolism to the defense one, leading to sequential growth defects of plants. Taken together, NAD homeostasis serves as one critical metabolic checkpoint surveilling plant growth and defense and can trigger multi-layer defense, especially when NAD^+ is depleted in plants.

Methods

Plant materials

The *Arabidopsis thaliana* genetic materials used in this study are in the Columbia-0 background. The complementation lines (COM1, COM2) of *qs-2*, and mutants including *qs-2*, *rbohF3*, *qs-2rbohF3* were described in our previous study[8]. The *coi1-2* and *aos* mutants were kindly provided by Prof. Yang Bai (Peking University), and the homozygous double mutant *qs-2coi1-2* was generated by genetic cross. The overexpression lines of *AtBGLU28* and CRISPR knockout materials including *lox2-c1/2*, *qs-2lox2-c1/2*, *qs-2aos*, *qs-2myb2829-1*, *qs-2myb2829-2*, *qs-2myb3451-2* and *qs-2myb3451-4* were generated for the first time in this work. For seedlings grown in Petri dishes, seeds were surface-sterilized and stored in sterile water at 4 °C for 48 h, then sown on half strength Murashige and Skoog (1/2 MS) medium (pH5.8) containing 1% (w/v) sucrose and 0.6% (w/v) agar. For plants grown in soils, 7-day-old seedlings grown in agar plates were transplanted to potting soil and grown in a growth room at 22 °C with 16 h light/8 h dark (long day condition) or 10 h light/14 h dark (short day condition), unless specified otherwise.

To obtain the homozygous CRISPR knockout lines, we designed a 19 bp single-guide RNA (sgRNA) with PAM (NGG) for each gene and cloned into the binary vector as described previously[44]. These constructs were transformed into *Agrobacterium* stain GV3101 for transfection of Col-0 or *qs-2* plants using the floral dip method[45]. The homozygous knockout lines were isolated and identified by PCR-based sequencing. The *35S:BGLU28-YFP* fusion was constructed by inserting the full-length coding sequence of *BGLU28* into a modified pCambia1300-N1-YFP vector with the 35S promoter, which was then transformed into *qs-2* mutant plants. The T4 homozygous transgenic seedlings were selected and used for further analysis. For transient expression of the TIR domain of HsSARM1 protein, the coding sequence of HsSARM1-TIR was amplified form cDNA of mammalian cells and cloned into the modified pCambia1300-35S: YFP vector. This construct was introduced into *Agrobacterium* stain GV3101 for transfection and expression in *N. benthamiana* leaves. The primers used were listed in the Supplementary Table 2.

RNA-sequencing and transcriptome analysis

Rosette leaves of 21-day-old Col-0 wild-type and *qs-2* mutant plants grown in soils were collected for total RNA extraction using a Total RNA Extraction Kit (Hua Yue Yang). The purified total RNA of high-quality was used to construct cDNA libraries for RNA-seq using NEBNext® UltraTM RNA Library Prep Kit for Illumina® (NEB, USA) following manufacturer's instructions. After quality control analysis, the cDNA libraries were sequenced on Illumine Nova platform, and 150 bp pair-end raw reads were generated for each sample. Three independent biological replicates were used for RNA sequencing.

The sequencing raw reads were filtered by removing the sequencing adapters and low-quality reads with 18 bp trimmed in front of the raw reads to obtain clean reads using fastp[46]. The clean reads were mapped to the *A. thaliana* reference genome TAIR10 using HISAT (hierarchical indexing for spliced alignment of transcripts)[47]. With these mapped reads in each sample, featureCounts[48] was used to calculate the raw read counts for each gene. Differentially expressed genes were identified by DEseq2[49]. Genes with an adjusted p value ($p$adj) < 0.05 and |Log2FC (*qs-2*/Col-0)| ≥ 2 were considered as significant differential expression genes (DEGs) between *qs-2* and Col-0. The KEGG enrichment analysis for upregulated and down-regulated DEGs were carried out via the clusterProfiler R package[50]. The GO enrichment analysis was conducted using Metascape[51].

Gene expression analysis

To examine the transcript levels of genes involved in the biosynthesis of jasmonates and glucosinolates, mature rosette leaves from 3-week-old plants grown in soil under short day condition were harvested for analysis. For verifying the expression of *BGLU28* in the overexpression plants, 10-day-old seedlings of the indicated genotypes grown in 1/2 MS plates were collected for analysis. Total RNA was extracted with Quick RNA Isolation Kit (Hua Yue Yang) and cDNA synthesized using One-Step gDNA Removal and cDNA Synthesis Supermix (TransGen Biotech). All quantitative real-time PCR analyses in this study were performed in a CFX96 Real-time system (Bio-Rad) using the ChamQ SYBR qPCR Master Mix (Vazyme Biotech) following the manufacturer's protocol. *ACT2* (At3g18780) was used as an internal control, and primers used were listed in Supplementary Table 2.

Immunoblot analysis

Immunoblot analysis was conducted as described previously[52]. In brief, rosette leaves from 21-day-old *A. thaliana* plants were collected for extraction of total proteins. Total proteins were extracted using the extraction buffer (50 mM Tris-HCl, pH8.0; 400 mM NaCl; 0.5% (v/v) Nonidet P-40; 10% (v/v) glycerol; 1 mM EDTA; 1 mM dithiothreitol; and

1 mM phenylmethylsulfonyl fluoride), separated in a 10% SDS-PAGE gel and electroblotted to NC membrane (Millipore). The abundance of LOX2 was determined using the anti-LOX2 antibody (No. PHY2142S, PhytoAB), and BGLU28-YFP fused proteins detected with anti-GFP antibody (No. 11814460001, Roche).

Histochemical staining

Hydrogen peroxide (H_2O_2) and superoxide anion (O_2^-) were detected using DAB and NBT staining, respectively as previously described[53]. For DAB staining, the expended leaves of 3-weeks-old plants were collected and stained for 24 h in a dye buffer containing 1 mg/mL DAB (Sangon Biotech), 0.1 M potassium phosphate buffer, pH7.0 and 0.1% (v/v) Triton X-100, and then fixed with a solution (3:1:1 v/v/v ethanol: lactic acid: glycerol) before being photographed. For NBT staining, rosette leaves were incubated in another buffer (0.1 M Tris-HCl, pH9.5, 0.1 M NaCl, 0.05 M $MgCl_2$, and 0.05% (v/v) Tween-20) containing 0.5 mg/mL NBT (Sangon Biotech) for 2 h. Singlet oxygen ($^1O_2$) was detected by 10 μM SOSG probes (Meilunbio, Dalian, China) and the same pairs of rosette leaves of each genotype were vacuum-infiltrated for 5 min according to those previously reported[54]. The fluorescence signal of $^1O_2$-activated SOSG was analyzed using confocal microscopy (TCS SP8, Leica Microsystems) with an excitation wavelength of 488 nm and an emission wavelength of 530 nm. At least six leaves from each genotype were used for the above histochemical staining assays and the staining intensity determined by ImageJ (version 1.50i).

Untargeted metabolomics analysis

Rosette leaves of 21-day-old Col-0 wild-type and *qs-2* mutant plants grown in soil were collected for untargeted metabolomics analysis. Briefly, rosette leaves of 21-day-old plants (100 mg fresh weight for each genotype) were extracted with 100% methanol (200 μL) with sonication for 30 min. The extraction was then centrifuged at 13,000 × *g* for 15 min. Finally, the 100 μL supernatant was used for liquid chromatography-mass spectrometry (LC-MS) analysis. LC-MS/MS analysis was carried out on a Thermo LC-MS Q Exactive-Orbitrap system (Thermo Fisher, paired with Vanquish UHPLC) equipped with a Kinetex C18 column (100 × 2.1 mm, 1.7 μm, 100 Å, Phenomenex). Milli-Q water containing 0.1% formic acid (solvent A) and acetonitrile (solvent B) were used as mobile phases, and all solvents used were LC-MS grade. The injection volume was 10 μL. The flow rate was set at 0.3 mL/min and column temperature at 35 °C. The capillary temperature was set at 320 °C and auxiliary gas heater temperature at 370 °C. The mass spectrometry (MS) data was acquired using a Thermo LC-MS Q Exactive-Orbitrap system in both positive and negative ionization modes. In positive mode, a heated electrospray ionization (HESI) source was employed with a full MS scan range set from 100 to 1000 *m/z*. Solvent gradient profile was as follows (% solvent B): 5% to 5% (0.0–1.5 min), 5% to 15% (1.5–15.0 min), 15% to 40% (15.0–25.0 min), 40% to 95% (25.0–43.0 min), 95% to 100% (43.0–48.5 min), 100% to 5% (48.5–49.0 min), and held at 5% for 1 min (49.0–50.0 min). In negative mode, the MS acquisition utilized a HESI source with a full MS scan range set from 300 to 600 *m/z*. Solvent gradient was as follows (solvent B%): 1% to 1% (0.0–5.0 min), 1% to 10% (5.0–7.0 min), 10% (7.0–8.5 min), 10% to 20% (8.5–10.5 min), 20% to 100% (10.5–15.0 min), 100% (15.0–18.0 min), 100% to 1% (18.0–19.0 min), and held at 1% for 1 min (19.0–20.0 min).

The acquired data were analyzed with Compound Discovery 3.1.0 software (Thermo Fisher Scientific) with a built-in workflow for untargeted metabolomics analysis, including feature extraction, peak alignment, prediction of elemental composition, and feature annotation by query into databases including mzCloud, Chemspider and KEGG pathway. Principal component analysis (PCA) in multivariate statistic process and partial least squares-discriminant analysis (PLS-DA) were performed to compare the metabolic profiles among all samples using R packages mixOmics[55]. Differential metabolites were obtained based on their absolute $Log_2FC \geq 1$ and p value < 0.05 (Student's t test). KEGG annotation of compounds were conducted with in-house built R scripts and KEGG enrichment analysis of the differential metabolites between *qs-2* and Col-0 were performed with the MBROLE (http://csbg.cnb.csic.es/mbrole2/analysis.php)[56].

Targeted metabolomics analysis

For glucosinolate analysis, rosette leaves of 21-day-old plants grown in soil were harvested and quickly frozen in liquid nitrogen. The samples were lyophilized and approximately 40 mg of each sample was extracted with 70% methanol (in ddH_2O) with sonication for 30 min, and analyzed by LC-MS as described previously[57]. Briefly, 10 μL of sample was injected into the LC-MS system (Q-Exactive-Orbitrap, Thermo Scientific) equipped with a Kinetex C18 column (100 × 2.1 mm, 1.7 μm, 100 Å, Phenomenex) and eluted with solvent gradient specified *vide infra* [solvent A (0.1% formic acid in Milli-Q water) and solvent B (acetonitrile)]. The flow rate was set at 0.3 mL/min and column temperature at 35 °C. The capillary temperature was set at 320 °C and auxiliary gas heater temperature was set at 370 °C. Solvent gradient was as follows (solvent B%): 1% to 1% (0.0–5.0 min), 1% to 10% (5.0–7.0 min), 10% (7.0–8.5 min), 10% to 20% (8.5–10.5 min), 20% to 100% (10.5–15.0 min), 100% (15.0–18.0 min), 100% to 1% (18.0–19.0 min), and 1% for 1 min (19.0–20.0 min). The MS data were acquired in negative mode under HESI source with full MS scan range set at 100–1000 *m/z*. The Full-MS/ddMS2 (data dependent MS/MS) mode was applied to acquire high-quality MS2 data with 35 eV normalized collision energy. Glucosinolates were identified by comparing their relative retention times, accurate masses, and mass fragmentation patterns with those of the standards or previous reported data[48]. GSL standards used in this study including indolyl-3-methyl glucosinolate (I3M, No. HB-07722), 4-methoxy-indol-3-ylmethyl glucosinolate (4MOI3M, No. HB-00017), 4-hydroxy-3-indolylmethyl glucosinolate (4HOI3M, No. HB-202275), 3-butenylglucosinolate (4BTEY, No. HB-07720), 3-Methylsulfinylpropyl glucosinolate (3MSOP, No. HB-07717) and 4-methylsulfinylbutyl glucosinolate (4MOSB, No. HB-07705) were purchased from HerbRuler. Information regarding GSL characterization can be found in Supplementary Table 1.

To determine the contents of phytohormone JA (referred to (+)-7-*iso*-JA), JA-Ile (referred to (+)-7-*iso*-JA-Ile) and its biosynthetic intermediates including α-linolenic acid (α-LeA), 13(S)-hydroperoxide (13-HPOT) and 12-oxo-phytodienoic acid (referred to *cis*-(+)-OPDA, 12-OPDA), leaf samples (100 mg fresh weight for each) from 3-week-old *A. thaliana* or 5-week-old *N. benthamiana* plants were collected. JA and its intermediates were extracted and quantified with previously described method with slight modifications[58]. Authentic standards of the above chemicals were ordered from the following suppliers: JA (CAS: 62653-85-4, No. 88320) from Cayman, JA-Ile (CAS: 120330-92-9, No. J210560) from TRC, α-LeA (CAS: 463-40-1, No. M184622) from Mreda, 13-HPOT (CAS: 67597-26-6, No. C5493) from APExBIO, and 12-OPDA (CAS: 85551-10-6, No. GC41888) from GLPBIO. Briefly, 10 μL of the sample was injected into the LC-MS system with mass spec setup similar to the glucosinolate analysis method. Solvent gradient was as follows (solvent B%): 5% (0.0–0.3 min), 5% to 35% (0.3–3.0 min), 35% to 60% (3.0–10.5 min), 60% to 100% (10.5–11.5 min), 100% (11.5–13.5 min) and 100% to 5% (13.5–13.6 min), equilibrating 5% for 1.4 min (13.6–15.0 min). The MS data were acquired in negative ion mode with scan range set at 100–360 *m/z*.

The analysis of chlorophyll content was performed as previously described[8]. Briefly, the chlorophyll was extracted from 3-week-old leaves using 80% (v/v) acetone. The supernatant was collected by centrifugation at 12,000 × *g* for 10 min at 4 °C, and then the absorption at 645 and 663 nm was measured using a NanoDrop 2000C spectrophotometer (Thermo Fisher Scientific).

To determine the contents of pyridine nucleotides, including NAD(H) and NADP(H), rosette leaves of 3-week-old *A. thaliana* plants

(with or without NA treatment) were harvested. The contents of pyridine nucleotides were determined by the enzyme-cycling assay as described previously[59]. Briefly, 100 mg of fresh *A. thaliana* leaves were grinded in liquid nitrogen followed by addition of 500 µL buffer (0.1 M $HClO_4$ for NAD^+ and NADP extraction, 0.1 M KOH for NADH and NADPH extraction). The supernatants were collected after centrifugation at 12,000 × *g* at 4 °C for 10 min. The samples were incubated on ice for 30 min, then at 95 °C for 10 min, followed by cooling down on ice. After adding 50 µL of detection mix buffer, the absorbance at 570 nm at 30 °C was recorded using the micro-plate reader (SpectraMax® i3x, Molecular Devices). The analysis of NAD and its degraded product cADPR in *A. thaliana* or *N. benthamiana* plants was performed as previously described with slight modifications[3]. Leaves from 3-week-old *A. thaliana* or 5-week-old *N. benthamiana* plants were harvested, and NAD and cADPR were extracted with 50% aqueous acetonitrile and determined using LC-MS with a ZORBAX Extend C18 column (100 mm × 2.1 mm internal diameter, 1.8 µm; Agilent, USA). Solvent gradient was as follows (solvent B%): 1% (0.0–1.0 min), 1% to 5% (1.0–4.0 min), 5% to 98% (4.0–4.1 min), 98% (4.1–5.0 min) and 98% to 1% (5.0–5.1 min), equilibrating 1% for 0.9 min (5.1–6.0 min). The MS data were acquired in positive ion mode with scan range set at 100-700 m/z. The content of NAD^+ was quantified based on calibration curves of commercially available authentic standard (No. N111610, Aladdin), and cADPR was determined and quantified based on MS^2 data. The Parallel-reaction monitoring (PRM) mode was applied to acquire MS^2 data of cADPR [$(M+H)^+ = 542.06839$, 542 > 136, 542 > 348].

Analysis of chlorophyll fluorescence

For determination of photochemical efficiency (*Fv*/*Fm*), 7-day-old seedlings of *qs-2*, COM1 and Col-0 wild-type plants were transferred to soil and grown for additional 3–4 weeks. The mature rosette leaves of plants were then used to detect the *Fv*/*Fm* values using a portable fluorometer Junior-PAM (Walz, Germany) as described in the manufacturer's instructions.

Plant treatments

For nicotinic acid (NA) treatment, 7-day-old seedlings in agar plates were transferred to soil and grown in a growth room at 22 °C with short day condition for additional 7 days. On the 8th day, the plants were supplemented with 1 mM NA in water for 10 days, after which the leaf area was calculated and the rosette leaves collected for metabolite and gene expression analysis. For exogenous supplement of DBS (Mreda, CAS: 270573-71-2) or DCMU (Aladdin, CAS:330-54-1), 3-week-old plants grown in the aforementioned normal condition were sprayed with 10 mM DBS or 200 µM DCMU for the indicated time lengths, and the rosette leaves collected for further analysis. The levels of $^1O_2$ after DBS treatment were determined using a singlet oxygen detection kit according to the instructions provided by the supplier (Shanghai BestBio).

For insect resistance test, the insect culture and feeding experiments were performed as previously described[60]. Briefly, the eggs of cotton bollworm (*Helicoverpa armigera*) were obtained and the larvae were reared in a growth chamber at 25 °C with 70% relative humidity and 14 h light/10 h dark. Second-instar or third-instar larvae of *H. armigera* at synchronous later stage were weighed individually before insect feeding assay, and larvae were divided into groups with each containing 24–36 individuals for the indicated genotypes. Four-week-old plants grown in soil were harvested for feeding *H. armigera* and the larva were replenished with fresh plants once a day. The weight increases were recorded after feeding with the designated diets for indicated days. For analyzing the insect preference, 7-day-old seedlings of Col-0, *qs-2*, COM1 and BGLU28-OE2 were transferred to soil and grown in a same pot for another 2–3 weeks, following by infestation of six synchronous third instar larvae of *H. armigera*. The photograph recoded before and after treatment were represented the leaf damage.

Statistics and reproducibility

Data are presented as mean ± SD. The Significance analysis was performed by two-tailed Student's *t* test conducted using R or Excel. The sample sizes (*n*) chosen were appropriate for the statistical analyses, and *p* values and sample sizes (*n*) are indicated and described in individual figures and Supplementary Figs. and the relevant legends. No data were excluded. The design and data collection of experiments were randomized. The results of all key experiments were reproducibly confirmed. Source data are provided as a Source Data file.

Reporting summary

Further information on research design is available in the Nature Portfolio Reporting Summary linked to this article.

Data availability

The experiment data that support the findings of this study are available from the corresponding author upon reasonable request. The RNA-seq data from this study have been deposited to the NCBI Gene Expression Omnibus repository database under the Bio-project accession number PRJNA986676. The metabolomics data generated in this study have been deposited in the MetaboLights database under accession code MTBLS10564. Source data are provided with this paper.

References

1. Huot, B., Yao, J., Montgomery, B. L. & He, S. Y. Growth-defense tradeoffs in plants: a balancing act to optimize fitness. *Mol. Plant* **7**, 1267–1287 (2014).
2. Waadt, R. et al. Plant hormone regulation of abiotic stress responses. *Nat. Rev. Mol. Cell Biol.* **23**, 680–694 (2022).
3. Hashida, S.-N., Takahashi, H. & Uchimiya, H. The role of NAD biosynthesis in plant development and stress responses. *Ann. Bot.* **103**, 819–824 (2009).
4. Smith, E. N., Schwarzlander, M., Ratcliffe, R. G. & Kruger, N. J. Shining a light on NAD- and NADP-based metabolism in plants. *Trends Plant Sci.* **26**, 1072–1086 (2021).
5. Feitosa-Araujo, E., da Fonseca-Pereira, P., Knorr, L. S., Schwarzlander, M. & Nunes-Nesi, A. NAD meets ABA: connecting cellular metabolism and hormone signaling. *Trends Plant Sci.* **27**, 16–28 (2022).
6. Petriacq, P., Ton, J., Patrit, O., Tcherkez, G. & Gakiere, B. NAD acts as an integral regulator of multiple defense layers. *Plant Physiol.* **172**, 1465–1479 (2016).
7. Wei, M. et al. The cloning and characterization of hypersensitive to salt stress mutant, affected in quinolinate synthase, highlights the involvement of NAD in stress-induced accumulation of ABA and proline. *Plant J.* **102**, 85–98 (2020).
8. Hong, Y. et al. Reciprocal regulation between nicotinamide adenine dinucleotide metabolism and abscisic acid and stress response pathways in Arabidopsis. *PLoS Genet.* **16**, e1008892 (2020).
9. Petriacq, P. et al. Inducible NAD overproduction in Arabidopsis alters metabolic pools and gene expression correlated with increased salicylate content and resistance to Pst-AvrRpm1. *Plant J.* **70**, 650–665 (2012).
10. Gakière, B. et al. NAD+ biosynthesis and signaling in plants. *Crit. Rev. Plant Sci.* 1–49, https://doi.org/10.1080/07352689.2018.1505591 (2018).
11. Katoh, A., Uenohara, K., Akita, M. & Hashimoto, T. Early steps in the biosynthesis of NAD in Arabidopsis start with aspartate and occur in the plastid. *Plant Physiol.* **141**, 851–857 (2006).
12. Hunt, L., Lerner, F. & Ziegler, M. NAD—new roles in signalling and gene regulation in plants. *N. Phytol.* **163**, 31–44 (2004).

13. Hashida, S. N., Takahashi, H., Kawai-Yamada, M. & Uchimiya, H. Arabidopsis thaliana nicotinate/nicotinamide mononucleotide adenyltransferase (AtNMNAT) is required for pollen tube growth. *Plant J.* **49**, 694–703 (2007).
14. Wu, R. et al. MeNA, controlled by reversible methylation of nicotinate, is an NAD precursor that undergoes long-distance transport in Arabidopsis. *Mol. Plant* **11**, 1264–1277 (2018).
15. Halkier, B. A. & Gershenzon, J. Biology and biochemistry of glucosinolates. *Annu. Rev. Plant Biol.* **57**, 303–333 (2006).
16. Bednarek, P. et al. A glucosinolate metabolism pathway in living plant cells mediates broad-spectrum antifungal defense. *Science* **323**, 101–106 (2009).
17. Clay, N. K., Adio, A. M., Denoux, C., Jander, G. & Ausubel, F. M. Glucosinolate metabolites required for an Arabidopsis innate immune response. *Science* **323**, 95–101 (2009).
18. Sugiyama, R. et al. Retrograde sulfur flow from glucosinolates to cysteine in Arabidopsis thaliana. *Proc. Natl Acad. Sci. USA*. **118**, https://doi.org/10.1073/pnas.2017890118 (2021).
19. Sonderby, I. E., Burow, M., Rowe, H. C., Kliebenstein, D. J. & Halkier, B. A. A complex interplay of three R2R3 MYB transcription factors determines the profile of aliphatic glucosinolates in Arabidopsis. *Plant Physiol.* **153**, 348–363 (2010).
20. Frerigmann, H. & Gigolashvili, T. MYB34, MYB51, and MYB122 distinctly regulate indolic glucosinolate biosynthesis in Arabidopsis thaliana. *Mol. Plant* **7**, 814–828 (2014).
21. Mitreiter, S. & Gigolashvili, T. Regulation of glucosinolate biosynthesis. *J. Exp. Bot.* **72**, 70–91 (2021).
22. Burow, M. et al. The glucosinolate biosynthetic gene AOP2 mediates feed-back regulation of jasmonic acid signaling in Arabidopsis. *Mol. Plant* **8**, 1201–1212 (2015).
23. Guo, R. et al. Jasmonic acid and glucose synergistically modulate the accumulation of glucosinolates in Arabidopsis thaliana. *J. Exp. Bot.* **64**, 5707–5719 (2013).
24. Yan, J. et al. The Arabidopsis CORONATINE INSENSITIVE1 protein is a jasmonate receptor. *Plant Cell* **21**, 2220–2236 (2009).
25. von Malek, B., van der Graaff, E., Schneitz, K. & Keller, B. The Arabidopsis male-sterile mutant dde2-2 is defective in the ALLENE OXIDE SYNTHASE gene encoding one of the key enzymes of the jasmonic acid biosynthesis pathway. *Planta* **216**, 187–192 (2002).
26. Wasternack, C. & Song, S. Jasmonates: biosynthesis, metabolism, and signaling by proteins activating and repressing transcription. *J. Exp. Bot.* **68**, 1303–1321 (2017).
27. Chauvin, A., Lenglet, A., Wolfender, J. L. & Farmer, E. E. Paired hierarchical organization of 13-lipoxygenases in Arabidopsis. *Plants* **5**, https://doi.org/10.3390/plants5020016 (2016).
28. Porta, H. & Rocha-Sosa, M. Plant lipoxygenases. Physiological and molecular features. *Plant Physiol.* **130**, 15–21 (2002).
29. Sasaki, Y. et al. Monitoring of methyl jasmonate-responsive genes in Arabidopsis by cDNA macroarray: self-activation of jasmonic acid biosynthesis and crosstalk with other phytohormone signaling pathways. *DNA Res.* **8**, 153–161 (2001).
30. Wasternack, C. & Hause, B. Jasmonates: biosynthesis, perception, signal transduction and action in plant stress response, growth and development. An update to the 2007 review in Annals of Botany. *Ann. Bot.* **111**, 1021–1058 (2013).
31. Krieger-Liszkay, A. Singlet oxygen production in photosynthesis. *J. Exp. Bot.* **56**, 337–346 (2005).
32. Flors, C. et al. Imaging the production of singlet oxygen in vivo using a new fluorescent sensor, Singlet Oxygen Sensor Green. *J. Exp. Bot.* **57**, 1725–1734 (2006).
33. Kim, M. et al. Colorimetric determination of singlet oxygen scavengers using a protein photosensitizer. *BioChip J.* **14**, 148–157 (2020).
34. Jannah, F., Lee, J., Seong, H.-J., Kim, J.-M. & Kim, Y.-P. A photodynamic color sensor using diacetylene vesicles for the rapid visualization of singlet oxygen. *Sens. Actuators B. Chem.* **380**, 133336 (2023).
35. Siedow, N. J. Plant lipoxygenase: structure and function. *Annu. Rev. Plant. Physiol. Plant. Mol. Biol.* **42**, 145–188 (1991).
36. Przybyla, D. et al. Enzymatic, but not non-enzymatic, 1O2-mediated peroxidation of polyunsaturated fatty acids forms part of the EXECUTER1-dependent stress response program in the flu mutant of Arabidopsis thaliana. *Plant J.* **54**, 236–248 (2008).
37. Wan, L. et al. TIR domains of plant immune receptors are NAD(+)-cleaving enzymes that promote cell death. *Science* **365**, 799–803 (2019).
38. Horsefield, S. et al. NAD(+) cleavage activity by animal and plant TIR domains in cell death pathways. *Science* **365**, 793–799 (2019).
39. Hunziker, P. et al. Herbivore feeding preference corroborates optimal defense theory for specialized metabolites within plants. *Proc. Natl Acad. Sci. USA* **118**, https://doi.org/10.1073/pnas.2111977118 (2021).
40. Jeschke, V. et al. How glucosinolates affect generalist lepidopteran larvae: growth, development and glucosinolate metabolism. *Front. Plant Sci.* **8**, 1995 (2017).
41. Chen, S. et al. CYP79F1 and CYP79F2 have distinct functions in the biosynthesis of aliphatic glucosinolates in Arabidopsis. *Plant J.* **33**, 923–937 (2003).
42. Zhao, Y. et al. Trp-dependent auxin biosynthesis in Arabidopsis: involvement of cytochrome P450s CYP79B2 and CYP79B3. *Genes Dev.* **16**, 3100–3112 (2002).
43. Zhang, X. & Mou, Z. Extracellular pyridine nucleotides induce PR gene expression and disease resistance in Arabidopsis. *Plant J.* **57**, 302–312 (2009).
44. Wang, Z. P. et al. Egg cell-specific promoter-controlled CRISPR/Cas9 efficiently generates homozygous mutants for multiple target genes in Arabidopsis in a single generation. *Genome Biol.* **16**, 144 (2015).
45. Clough, S. J. & Bent, A. F. Floral dip: a simplified method for Agrobacterium-mediated transformation of Arabidopsis thaliana. *Plant J.* **16**, 735–743 (1998).
46. Chen, S., Zhou, Y., Chen, Y. & Gu, J. fastp: an ultra-fast all-in-one FASTQ preprocessor. *Bioinformatics* **34**, i884–i890 (2018).
47. Kim, D., Langmead, B. & Salzberg, S. L. HISAT: a fast spliced aligner with low memory requirements. *Nat. Methods* **12**, 357–360 (2015).
48. Liao, Y., Smyth, G. K. & Shi, W. featureCounts: an efficient general purpose program for assigning sequence reads to genomic features. *Bioinformatics* **30**, 923–930 (2014).
49. Love, M. I., Huber, W. & Anders, S. Moderated estimation of fold change and dispersion for RNA-seq data with DESeq2. *Genome Biol.* **15**, 550 (2014).
50. Yu, G., Wang, L. G., Han, Y. & He, Q. Y. clusterProfiler: an R package for comparing biological themes among gene clusters. *OMICS* **16**, 284–287 (2012).
51. Zhou, Y. et al. Metascape provides a biologist-oriented resource for the analysis of systems-level datasets. *Nat. Commun.* **10**, 1523 (2019).
52. Hong, Y. et al. Two chloroplast proteins negatively regulate plant drought resistance through separate pathways. *Plant Physiol.* **182**, 1007–1021 (2020).
53. Wang, Z. et al. Two chloroplast proteins suppress drought resistance by affecting ROS production in guard cells. *Plant Physiol.* **172**, 2491–2503 (2016).
54. Ramel, F. et al. Chemical quenching of singlet oxygen by carotenoids in plants. *Plant Physiol.* **158**, 1267–1278 (2012).
55. Rohart, F., Gautier, B., Singh, A. & Le Cao, K. A. mixOmics: an R package for 'omics feature selection and multiple data integration. *PLoS Comput. Biol.* **13**, e1005752 (2017).
56. Lopez-Ibanez, J., Pazos, F. & Chagoyen, M. MBROLE 2.0-functional enrichment of chemical compounds. *Nucleic Acids Res.* **44**, W201–204, (2016).

57. Hwang, I. M., Park, B., Dang, Y. M., Kim, S. Y. & Seo, H. Y. Simultaneous direct determination of 15 glucosinolates in eight Brassica species by UHPLC-Q-Orbitrap-MS. *Food Chem.* **282**, 127–133 (2019).
58. Pan, X., Welti, R. & Wang, X. Quantitative analysis of major plant hormones in crude plant extracts by high-performance liquid chromatography-mass spectrometry. *Nat. Protoc.* **5**, 986–992 (2010).
59. Zhang, Y., Krahnert, I., Bolze, A., Gibon, Y. & Fernie, A. R. Adenine nucleotide and nicotinamide adenine dinucleotide measurements in plants. *Curr. Protoc. Plant Biol.* **5**, e20115 (2020).
60. Chen, C. Y. et al. An effector from cotton bollworm oral secretion impairs host plant defense signaling. *Proc. Natl Acad. Sci. USA* **116**, 14331–14338 (2019).

Acknowledgements

We thank Prof. Yang Bai (Peking University) for providing the *coi1-2* and *aos* mutants, Dr. Minjie Cao (Southern University of Science and Technology) and Prof. Xiangqiang Zhan (Northwest A&F University) for their helpful discussions and suggestions to this work. We acknowledge the technical support from the SUSTech Core Research Facilities (CRF) for microscopic analysis, and the mass spectrometry platform of SUSTech-PKU Institute of Plant and Food Science for LC-MS analysis. This work has been supported by the National Science Foundation of China (grant no. 32200234 to Yechun Hong; 32370298 to A.C.H.), Shenzhen Science and Technology Program (grant no. RCBS20210706092213009 to Yechun Hong; ZDSYS20230626091659010 to H.G. and A.C.H.; KCXFZ20211020174802004 to A.C.H.), Scientific research funding for postdoctoral researchers staying at Shenzhen (grant no. K231227503 to Yechun Hong), the China Postdoctoral Science Foundation (grant no. 2021M691430 to Yechun Hong), the SUSTech Presidential Postdoctoral Fellowship (to Yechun Hong), Shenzhen Municipal Startup Fund (to A.C.H.). The schematic and working model presented in Fig. 6 were created via BioRender.com.

Author contributions

Yechun Hong and A.C.H. conceived and supervised the project. Yechun Hong designed the experiments. Yechun Hong and Z.Y. performed most of the experiments and analyzed the data. Q.Z. analyzed the transcriptomics and untargeted metabolomics data. C.C., Yuqiong Hao and Z.W. provided technical assistances. Yechun Hong and A.C.H. drafted the manuscript. Yechun Hong, J.-K.Z., H.G. and A.C.H. revised the manuscript.

Competing interests

The authors declare no competing interests.

Additional information

Supplementary information The online version contains supplementary material available at https://doi.org/10.1038/s41467-024-51114-1.

Correspondence and requests for materials should be addressed to Ancheng C. Huang.

Peer review information *Nature Communications* thanks the anonymous, reviewer(s) for their contribution to the peer review of this work. A peer review file is available.

Reprints and permissions information is available at http://www.nature.com/reprints

Publisher's note Springer Nature remains neutral with regard to jurisdictional claims in published maps and institutional affiliations.

Open Access This article is licensed under a Creative Commons Attribution-NonCommercial-NoDerivatives 4.0 International License, which permits any non-commercial use, sharing, distribution and reproduction in any medium or format, as long as you give appropriate credit to the original author(s) and the source, provide a link to the Creative Commons licence, and indicate if you modified the licensed material. You do not have permission under this licence to share adapted material derived from this article or parts of it. The images or other third party material in this article are included in the article's Creative Commons licence, unless indicated otherwise in a credit line to the material. If material is not included in the article's Creative Commons licence and your intended use is not permitted by statutory regulation or exceeds the permitted use, you will need to obtain permission directly from the copyright holder. To view a copy of this licence, visit http://creativecommons.org/licenses/by-nc-nd/4.0/.

© The Author(s) 2024